



Cascaded crystalline Raman lasers for extended wavelength coverage: continuous-wave, third-Stokes operation

RICCARDO CASULA,^{1,*}  JUSSI-PEKKA PENTTINEN,²  MIRCEA GUINA,²  ALAN J. KEMP,¹
AND JENNIFER E. HASTIE¹

¹Institute of Photonics, Department of Physics, SUPA, University of Strathclyde, Technology and Innovation Centre, 99 George Street, Glasgow G1 1RD, UK

²Optoelectronic Research Centre, Tampere University of Technology, Korkeakoulunkatu 3, FIN-33101 Tampere, Finland

*Corresponding author: riccardo.casula@strath.ac.uk

Received 29 August 2018; revised 16 October 2018; accepted 16 October 2018 (Doc. ID 343021); published 2 November 2018

The development of high-power laser sources with narrow emission, tunable within the water transmission window around 1.7 μm , is of interest for applications as diverse as medical imaging and atmospheric sensing. Where suitable laser gain media are not available, operation in this spectral region is often achieved via nonlinear frequency conversion, and optical parametric oscillators (OPOs) are a common solution. A practical alternative to OPOs, to avoid birefringent- or quasi-phase-matching requirements, is the use of stimulated Raman scattering within a suitable material to convert a pump source to longer wavelengths via one or more Stokes shifts; however, as this is a $\chi^{(3)}$ nonlinear process, such frequency conversion is usually the preserve of high-energy pulsed lasers. Semiconductor disk lasers (SDLs), on the other hand, have very high-finesse external resonators, suitable for efficient intracavity nonlinear conversion even in continuous-wave (CW) operation. Here we report, to the best of our knowledge, the first continuous-wave third-Stokes crystalline Raman laser and the longest emission wavelength from an SDL-pumped Raman laser, achieving high power, CW output, and broad wavelength tuning around 1.73 μm . The $\text{KGd}(\text{WO}_4)_2$ (KGW) Raman laser, which was intracavity-pumped by a 1.18 μm InGaAs-based SDL, demonstrated cascaded CW Stokes oscillation at 1.32 μm , 1.50 μm , and 1.73 μm with watt-level output achievable at each wavelength. The 1.73 μm Stokes emission was diffraction limited ($M^2 < 1.01$) and narrow linewidth (< 46 pm FWHM; measurement limited). By rotation of a birefringent filter placed within the fundamental resonator, we attained three tunable emission wavelength bands, one centred at each Stokes component, and achieved up to 65 nm tuning for the third-Stokes Raman laser from 1696 nm to 1761 nm. We have thus demonstrated a platform laser technology that takes well-developed InGaAs-based SDLs and provides spectral coverage and high performance in the near-infrared water transmission windows using commercially available components.

Published by The Optical Society under the terms of the [Creative Commons Attribution 4.0 License](https://creativecommons.org/licenses/by/4.0/). Further distribution of this work must maintain attribution to the author(s) and the published article's title, journal citation, and DOI.

<https://doi.org/10.1364/OPTICA.5.001406>

1. INTRODUCTION

Laser operation between 1.4 μm and 1.8 μm (the “eye-safe” region) is of interest for gas sensing [1], light detection and ranging (lidar) [2], and for medical imaging applications, e.g., optical coherence tomography (OCT) [3,4]. At around 1.7 μm in particular, there is a tissue (water) transmission window for which Rayleigh scattering and absorption are much lower than the more commonly used window at 1.3 μm [4,5]. (Indeed for this reason, a window centered at 1.73 μm has been reported as optimum for the imaging of brain tissue [6].) Likewise, there exists an atmospheric transmission window at ~ 1.5 –1.8 μm between bands of water vapor absorption. High brightness, narrow linewidth, broadly tunable lasers at 1.7 μm would enable parallel imaging

techniques, long-range sensing and lidar; however, the lack of practical sources at these wavelengths prevents wider take-up or further applications development. While InGaAsP-based semiconductor lasers such as distributed feedback lasers (DFBs) can emit directly at 1.7 μm , they are limited to low power (mW).

The expanding number of applications of semiconductor disk lasers (SDLs), also known as vertical-external-cavity surface-emitting lasers (VECSELs) [7], stems from their unique combination of laser properties, such as [8]: custom emission wavelength enabled by III-V semiconductor bandgap engineering, with broad tunability; output power at the multi-watt level with low noise and excellent beam quality; and suitability for short pulse (fs) mode locking or ultra-narrow linewidth (kHz)

single-frequency operation. SDLs typically consist of a multi-quantum-well (QW) gain region monolithically grown on top of a distributed Bragg reflector (DBR), which serves as the end mirror in an external laser resonator. Further, the extended cavity of the SDL enables efficient intracavity nonlinear conversion, which in turn extends spectral coverage to wavelengths where bandgap engineering is nontrivial. InGaAs QW SDLs are now well-established systems due to their high gain, high-quality AlGaAs DBRs, and suitability for pumping with efficient 808 nm diodes. Moreover, they can provide laser emission with tens of watts of output power and high beam quality in the region between ~ 920 nm and 1180 nm by tuning the indium content in the wells [9,10]. Operation of SDLs at wavelengths beyond 1.2 μm can be obtained with more challenging semiconductor epitaxy, such as the use of layers of InAs quantum dots (~ 1.25 μm [11]) or by adding nitrogen to the InGaAs QWs (up to ~ 1.55 μm [12,13]). Further, where monolithic growth on GaAs is no longer feasible, wafer fusion techniques have been developed that allow the fabrication of high-efficiency SDLs that emit directly in the eye-safe wavelength region (specifically at 1.3 μm , 1.48 μm , and 1.58 μm to date [14,15]). However, the complexity of such growth and fabrication has motivated further research into practical alternatives, such as the use of intracavity crystalline Raman media to Stokes-shift the emission wavelength of mature (commercialized), high-performance InGaAs SDLs [16–18], to close the gap towards monolithic GaSb-based SDLs (~ 1.9 – 3 μm [19]). Thus, a single-platform semiconductor laser technology could enable a broad range of applications from the blue (via second-harmonic generation) towards the mid-IR by changing commercially available intracavity optical components.

Stimulated Raman scattering, the basis of a Raman laser, is a practical approach by which a Raman gain medium can efficiently convert a pump laser source to longer wavelengths via characteristic Stokes shifts [20]. Further, even longer wavelengths can then be reached via cascaded Stokes shifts if the intensity of the Raman laser field is sufficiently high to further stimulate laser emission at the next-order Stokes wavelength [20]. Cascaded Raman conversion is routinely achieved via pumping with high-energy pulsed (*Q*-switched) lasers. Unlike OPOs, Raman lasers, based on a $\chi^{(3)}$ nonlinear process, do not require birefringent or quasi-phase matching, as there is always a phonon mode oscillating at the Raman frequency that conserves momentum.

Raman lasers have been demonstrated in pulsed or CW regimes using a broad range of crystalline media to access wavelengths beyond 1 μm , with diamond and $\text{KGd}(\text{WO}_4)_2$ (KGW) used to achieve high performance in several recent reports [17,20–24]. For instance, laser emission at 1.49 μm was demonstrated with diamond in a cascaded Raman laser, extracavity-pumped by a quasi-CW laser [25]. In the CW regime, we recently reported a Raman laser emitting at 1.4 μm achieved by first-Stokes generation in diamond within a 1.18 μm InGaAs SDL, achieving output power higher than 2 W with a spectral linewidth < 0.1 nm (FWHM) [26]. Wavelengths beyond 1.4 μm could be achieved with a similar setup via generation of cascaded higher-Stokes modes if the threshold condition for each Stokes-shifted field could be satisfied. The large Stokes shift of diamond (1332 cm^{-1}) would, in principle, enable a Raman laser at 1.72 μm with only two Stokes conversion steps. However, at the time of writing, most established optics manufactures have not yet

standardized robust deposition of anti-reflection (AR) coatings on diamond for such a wide wavelength range (1.18–1.72 μm), where reflection loss below $\sim 0.5\%$ per facet is generally required for an intracavity-pumping scheme.

In this work, we use a KGW crystal, with custom AR coatings ($R < 0.5\%$) optimized for cascaded Raman conversion up to the third-Stokes shift. KGW is a relatively common Raman crystal with relatively high gain on its 901 cm^{-1} Stokes shift, a high damage threshold (~ 10 GW/cm^2), and modest thermal conductivity (~ 3 $\text{Wm}^{-1}\text{K}^{-1}$) [27]. KGW has previously been investigated for cascaded Raman laser generation in the visible and near-IR via pumping with *Q*-switched lasers [21,28,29]; however, no CW demonstration at the third-Stokes has so far been reported, as pump power of several hundreds of Watts is required. Such power is readily achieved within the cavity of a diode-pumped SDL. Here we demonstrate a CW KGW cascaded Raman laser operating at 1.32 μm , 1.50 μm , and 1.73 μm , intracavity-pumped by a diode-pumped InGaAs SDL at around 1.18 μm . We achieve an output power greater than 6 W where the Raman laser is operating solely at the first-Stokes wavelength of 1.32 μm ; simultaneous output coupling of the first- and second-Stokes at 1.32 μm and 1.50 μm to give ~ 1 W at each wavelength; and a cascaded third-Stokes Raman laser, with output coupling at 1.73 μm only, to produce > 1 W output power, near diffraction-limited beam propagation, and a narrow spectral bandwidth < 46 pm FWHM. Tuning of the SDL oscillation wavelength resulted in broad tuning of each Raman laser, with up to 65 nm tuning achieved for the third-Stokes Raman laser from 1696 nm to 1761 nm.

2. EXPERIMENTAL SETUP AND RESULTS

A. SDL Characterization

The SDL gain mirror employed for this work was designed for oscillation around 1180 nm and contained 10 strain-compensated QWs of InGaAs/GaAs/GaAsP (37% indium fraction) grown monolithically on top of an AlGaAs DBR. Further details on the gain mirror can be found in Refs. [10,30]. SDL thermal management was achieved using an uncoated plane-parallel 500 μm thick diamond (Element Six Ltd.) as a heat spreader, bonded to the intracavity surface of the gain mirror via the liquid capillary technique [31]. The bonded gain mirror and diamond were clamped in a brass mount, cooled with a closed-cycle water chiller at 10°C .

Preliminary testing of the SDL gain mirror at 1180 nm was performed in a three-mirror cavity, consisting of the DBR as a plane end mirror, a highly reflective (HR) folding mirror [angle of incidence (AOI) $< 5^\circ$] with 200 mm radius of curvature and reflectivity $> 99.9\%$ from 1160 nm to 1190 nm, and a plane end mirror with 1.6% output coupling. The mirror separations were $\text{SDL} - \text{HR} = 110$ mm and $\text{HR} - \text{OC} = 200$ mm. The SDL gain mirror was pumped with a commercial fiber-coupled diode laser at 808 nm. External optics collimated and focused the beam to a spot radius of ~ 240 μm on the surface of the gain mirror with AOI $\sim 20^\circ$. After reflection losses at the surface of the diamond heat spreader, 80% of the pump power reaches the SDL gain mirror (hereafter referred to as absorbed pump power); however, this could be readily increased to close to 100% with an appropriate antireflection coating for the pump wavelength.

The free-running SDL reached threshold at 3 W of absorbed pump power and produced a maximum power of 17.8 W when

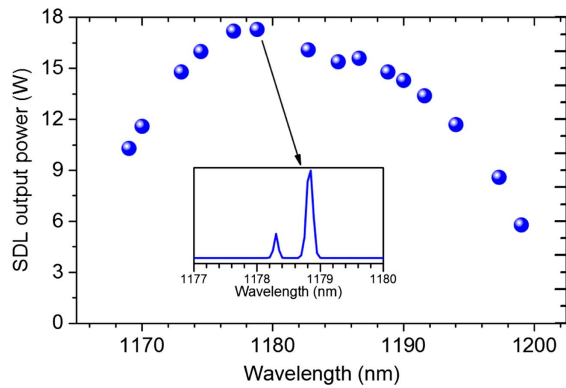


Fig. 1. Tuning curve of the SDL for 95 W absorbed pump power and 1.6% output coupling, obtained via rotation of an intracavity birefringent filter. Inset: SDL emission spectrum at the highest output power.

the absorbed pump was 102 W, beyond which thermal rollover was observed.

Figure 1 shows the SDL tuning curve obtained via in-plane rotation of an intracavity 4 mm thick birefringent filter (BRF), for 95 W absorbed pump power. The BRF narrowed the emission spectrum to <2 nm, and we achieved SDL tuning from 1170 nm to 1200 nm, limited by the free spectral range of the BRF, with maximum power at around 1179 nm. The SDL showed similar performance to the systems reported in Refs. [10,24].

B. SDL-Pumped KGW Raman Laser Setup

Figure 2 shows the experimental setup for the cascaded KGW Raman laser. Two partially shared four-mirror cavities were designed to resonate the fundamental (1.18 μm) and cascaded Raman wavelengths (1.32 μm , 1.50 μm , and 1.73 μm), respectively. The concave mirrors (M2, M3, and M4 in Fig. 3) were HR for all laser wavelengths ($R > 99.95\%$, 1150–1770 nm) and, along with the gain mirror, define the fundamental cavity; while M3, M4, a flat dichroic mirror (DM) and an output coupler (OC) define the Raman cavity. The DM, HR at the Raman wavelengths ($R > 99.9\%$) and highly transmissive at the fundamental ($T > 99\%$), was placed in the longest arm (M2–M3) with a folding angle of $<5^\circ$ in order to steer the Raman beam to the OC. Varying the distance between the DM and the OC allows optimization of the mode matching in the Raman crystal. Both resonators were designed to produce a ~ 41 μm TEM₀₀ beam waist radius in the center of the KGW. The 4 mm thick quartz BRF at Brewster's angle in the SDL cavity, outside the Raman resonator,

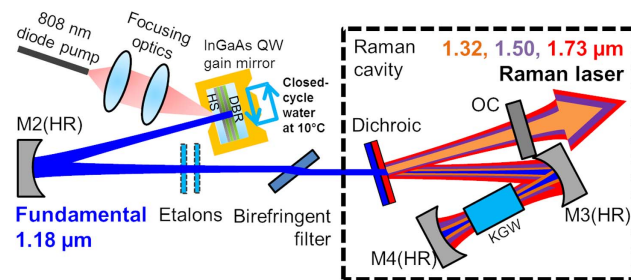


Fig. 2. Schematic of the SDL-pumped KGW Raman laser. HR, high reflector; OC, output coupler; DBR, distributed Bragg reflector; HS, heat spreader.

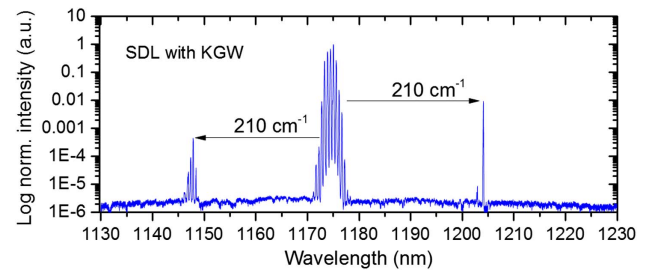


Fig. 3. Section of an emission spectrum of the intracavity-pumped KGW Raman laser obtained at high pump power.

had two functions: (i) to lock the polarization of the fundamental field and (ii) to tune the fundamental and hence the Raman laser wavelength. Two fused suprasil etalons with thicknesses of 50 μm and 500 μm were also available, with one or both inserted as required to further narrow the fundamental field, improving spectral overlap with the KGW Raman gain bandwidth. We used appropriate filtering in the output beams to allow separate characterization of the various Stokes orders.

C. KGW(VO₄)₂ Characterization

In this work we utilized a 30 mm long KGW crystal (EKSMA Optics) as the Raman gain medium, cut for propagation along the N_p axis and oriented to access the 901 cm^{-1} Raman shift via excitation along the N_m axis, maximizing the gain coefficient: $g_0 = 3.5$ cm/GW at 1064 nm [32]. To reduce the intracavity loss, both end faces (7 mm \times 7 mm) were coated for high transmission: $R < 0.5\%$ from 1160 nm to 1750 nm (LaserOptik). The KGW crystal was wrapped in indium foil and clamped into a brass mount. No active thermal management was implemented.

We measured reflectivities of 0.015% and 0.022% at 1180 nm for the two end facets of the crystal at normal incidence, with the corresponding total round-trip reflection loss calculated to be 0.074%. We also estimated the total insertion loss of the crystal at 1180 nm via Caird analysis by placing the crystal in the three-mirror SDL cavity and varying the output coupling [33]. By this method, the SDL cavity loss was $2.29 \pm 0.01\%$ per round trip, increased from $1.5 \pm 0.1\%$ without the KGW. Given the reflection loss of the KGW end surfaces, the remaining $0.79 \pm 0.05\%$ can be mostly attributed to the up-conversion process, quite common in KGW Raman lasers [34–36], which leads to blue photoluminescence, which was clearly observed both below and above the Raman laser threshold.

Up-conversion photoluminescence is, however, not the sole loss mechanism observed in KGW Raman lasers. As a low-symmetry crystal, KGW exhibits a number of weaker Raman features in addition to the 901 cm^{-1} shift for p[mm]p excitation [35]. The high-finesse resonator and high intracavity power in this work means multiple smaller Stokes shifts may occur and be parasitic for our target wavelength. Figure 3 shows an example of a spectrum acquired during fundamental p[mm]p excitation of the KGW when implemented in the high-finesse four-mirror resonator used for cascaded Raman conversion, taken using a fiber-coupled optical spectrum analyzer (OSA) with resolution 0.05 nm. The spectrum shows high-intensity, broad fundamental emission at ~ 1175 nm (multiple peaks with separation corresponding to the free spectral range of the diamond heat spreader),

and two other minor peaks at ~ 1145 nm and ~ 1205 nm, equally spaced by 210 cm^{-1} with respect to the fundamental. It is most likely that this Stokes shift corresponds to the Gd-O vibration in KGW as investigated in Ref. [35] and observed more recently in Ref. [22]. Therefore, it is probable that a slightly off-axis beam led to Stokes and anti-Stokes conversion in this case, though this was not always repeatable. Other possible Stokes shifts that were observed during optimization of the cascaded Raman laser will be highlighted in the following sections.

D. KGW Raman Laser Results

1. Anti-Stokes Laser (1060 nm)

The Raman cavity was first aligned with all HR mirrors (i.e., no output coupling) and no etalons to obtain all Raman wavelengths. Figure 4 shows a spectrum of the Raman laser at high pump power, obtained through the HR mirror leakage.

The fundamental wavelength of the SDL was Stokes-shifted to 1732 nm. The first-Stokes field is evident at 1320 nm. The second-Stokes field is presumed to oscillate at $1.5\text{ }\mu\text{m}$ in this case but was not visible in this measurement. We believe there are two factors that together make it difficult to detect this signal: first, the HR had very high reflectivity at $1.5\text{ }\mu\text{m}$, allowing little cavity leakage; and second, the second-Stokes intracavity field is expected to have low intensity compared with odd Stokes orders to allow sufficient first-Stokes oscillation, as per the cascaded-Stokes model in Ref. [37]. The anti-Stokes generation at 1066 nm was made possible by slight off-axis orientation of the Raman cavity to phase match the first-Stokes to the anti-Stokes photons. The anti-Stokes laser reached threshold at 28 W of absorbed diode pump power, just a few watts above the first-Stokes threshold. While adequate filters were not available to isolate the anti-Stokes beam for accurate power measurements, we note that the intensity, as analyzed by the spectrometer, was similar to that of the third-Stokes field. Also, the limited fine adjustment of the rotational stage of the KGW prevented direct control or optimization of the anti-Stokes, such that it was not systematically repeatable. Nevertheless, we report the first observation of a CW anti-Stokes laser pumped by an SDL.

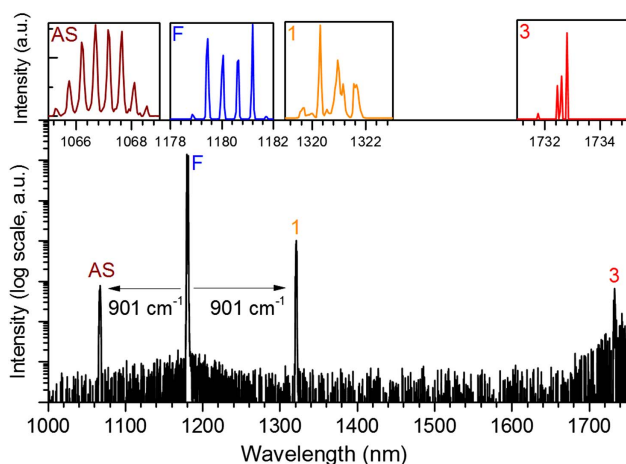


Fig. 4. Emission spectrum (0.2 nm resolution) of the SDL-pumped Raman laser for 92 W of absorbed diode pump power and an all-HR cavity. AS, anti-Stokes; F, fundamental; “1” and “3,” first- and third-Stokes lasers. Top insets: 0.05 nm resolution.

2. First-Stokes Laser (1300–1341 nm)

The Raman cavity was set up for high-power first-Stokes oscillation by using a 2.2% output coupling at $1.3\text{ }\mu\text{m}$, and no etalons. Up to 6.1 W output power at $1.32\text{ }\mu\text{m}$ with >80 W of absorbed pump power was achieved, as shown in Fig. 5. The Raman laser threshold was attained when the fundamental intracavity power reached ~ 300 W. Above the threshold, the output power of the Raman laser increased with a differential efficiency of 7.9% up to 70 W of pump power, increasing to 14% in the 70–80 W pump power range, above which the Raman laser saturated. Correspondingly, the fundamental intracavity power was nearly clamped above 70 W of pump power up to the rollover point at nearly 100 W. The irregular slope efficiency can be attributed to the interplay between thermal effects and spectral and spatial mode evolution over the range of the diode pump power.

Based on the performance of the SDL at 80 W absorbed pump power (16 W), we estimate the maximum effective fundamental to first-Stokes conversion efficiency of the Raman laser to be $>36\%$. This compares favorably to the previous report by Savitski *et al.* of a $1.14\text{ }\mu\text{m}$ KGW Raman laser, intracavity pumped by a Nd:YLF laser, with fundamental output of 18.4 W and first-Stokes output of 6.1 W (effective conversion efficiency 33%) for 150 W incident diode pump power [38].

The saturation of the Raman laser output power at 6 W could be due to the losses induced by thermal aberration caused by the heat deposited in the crystal during Raman conversion, although we do not exclude that some spatial and spectral overlap degradation and thermal roll-off of the SDL may have contributed as well. Indeed, while KGW has reasonably good thermal conductivity, 6 W of Raman output power can lead to a considerable thermal lens during Raman power extraction. Given the approximation in Ref. [39], we estimate the focal length of the thermal lens to be approximately -20 cm; however, this does not account for the possible compensating effect of end-face curvature.

We investigated the tuning curve of the Raman laser at high power, with 1% output coupling at $1.3\text{ }\mu\text{m}$ and the $50\text{ }\mu\text{m}$ thick etalon inserted for narrow emission. Figure 6 shows the wavelength tuning of the fundamental and Raman laser with the

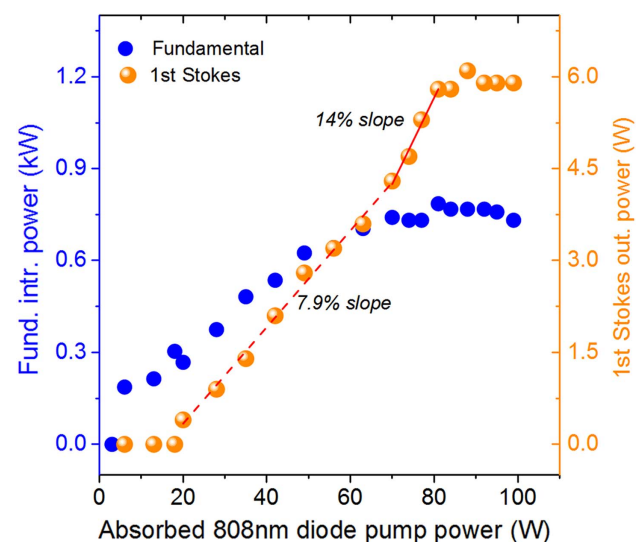


Fig. 5. Power transfer characteristic of the Raman laser and the fundamental intracavity power.

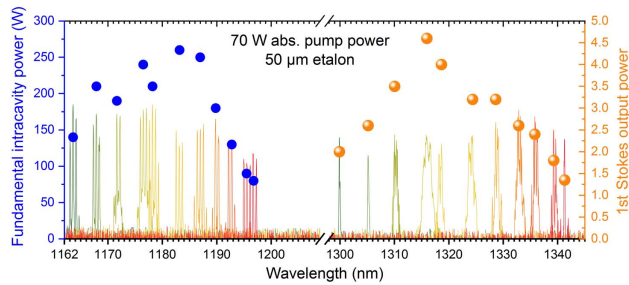


Fig. 6. Wavelength tuning of the fundamental laser (blue circles) with related tuning of the first-Stokes Raman laser (orange) at 70 W of absorbed diode pump power and corresponding log-scaled output spectra.

corresponding spectra at each power. Narrow laser emission of ~ 2 nm was obtained by rotating the BRF and simultaneously tilting the etalon. The etalon finesse was relatively low, such that a comb of a few Fabry–Perot peaks due to the diamond heat spreader emerged. The fundamental wavelength tuned from 1163 nm to 1196 nm, limited by the free spectral range of the BRF. The Raman laser wavelength was simultaneously tuned between 1300 nm and 1341 nm, i.e., each fundamental wavelength was Stokes-shifted by 901 cm^{-1} . The highest output power of 4.6 W was achieved when the Raman wavelength was 1316 nm, while pumped by the fundamental field at 1177 nm.

Sirbu *et al.* have previously demonstrated a wafer-fused, diamond-cooled SDL emitting at $1.3\text{ }\mu\text{m}$ with maximum output power of 7.1 W, pumped with a 980 nm diode laser [15]. Here, we have demonstrated a practical, alternative way to access the $1.32\text{ }\mu\text{m}$ window with similar power (and narrower linewidth) by taking an InGaAs SDL, which requires almost no post-processing, and achieving Raman conversion with a commercial KGW crystal. In the following section, we will show that this approach can be easily configured to shift the SDL operation to the $1.5\text{ }\mu\text{m}$ region via the second-Stokes shift.

3. Second-Stokes Laser (1470–1520 nm)

We achieved laser output at $1.5\text{ }\mu\text{m}$ using the same cavity configuration as shown in Fig. 2, now with an output coupler for both the first- and the second-Stokes-shifted fields, with transmission of 0.67% and 1%, respectively. Figure 7 shows the first- and

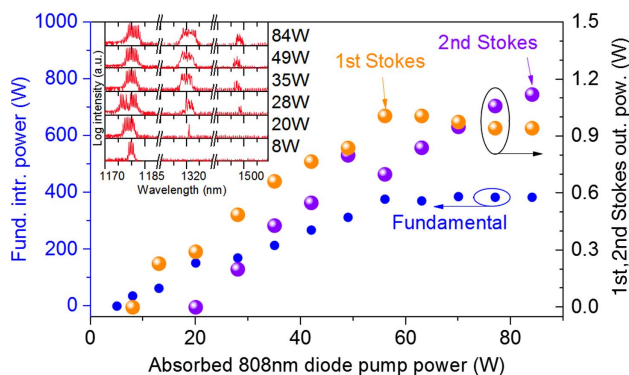


Fig. 7. Output power of the cascaded Raman at the first- and second-Stokes radiation (orange and purple spheres, respectively), and dependency of the fundamental intracavity power on the absorbed diode pump power (blue circles). Inset: Fundamental, first- and second-Stokes Raman spectra at different absorbed pump powers.

second-Stokes output power and fundamental intracavity power as a function of pump power. The Raman laser was optimized for high-power extraction at $1.5\text{ }\mu\text{m}$, and with 84 W of absorbed pump power we obtained a maximum power of 1.1 W at $1.5\text{ }\mu\text{m}$ and 0.9 W at $1.3\text{ }\mu\text{m}$. The fundamental power was clamped above nearly 60 W of pump power, where the first-Stokes output power slightly decreased. With no further filtering of the longitudinal modes (i.e., BRF only; no etalons), the fundamental and the first-Stokes linewidth widened to a maximum of ~ 5 nm at high power, while the second-Stokes reached a maximum of ~ 2 nm. A mirror with a customized coating, HR at the first-Stokes wavelength and output coupling at the second-Stokes wavelength only, was not available, but we expect that such a setup would lead to even higher output power at $1.5\text{ }\mu\text{m}$.

4. Third-Stokes Laser (1700–1760 nm)

The cascaded KGW Raman laser optimized for the third-Stokes wavelength was achieved using an output coupler coated for high reflectivity at the first- and second-Stokes wavelength ranges ($R > 99.95\%$) and with 1% transmission over 1660–1770 nm. In addition, the longest arm of the Raman cavity (OC-DM-M3; see Fig. 2) was adjusted to reduce the Raman cavity mode in the KGW to $36\text{ }\mu\text{m}$ at the first-Stokes wavelength for a lower Raman laser threshold.

Figures 8(a) and 8(b) show the power transfers of all four laser wavelengths with respect to the absorbed diode pump power and corresponding spectra evolution over the pump power range, taken with a resolution of 0.2 nm from 820 nm to 1750 nm. The third-Stokes laser reached a maximum output power of 1.1 ± 0.1 W for absorbed diode pump power of 84 W, well above the threshold of 50 W.

The laser at the third-Stokes emitted with a single peak located at 1731 nm with the use of two etalon filters, 50 and $500\text{ }\mu\text{m}$ thick, in the fundamental cavity. Figure 8(b) shows that the fundamental oscillates within a single peak in the pump power range of 60–84 W, with a second peak appearing at lower power. The Raman spectra exhibited minor Raman peaks located at 1283 nm and 1451 nm for an absorbed pump power higher than 60 W, which we tentatively ascribe to a 684 cm^{-1} Stokes shift of the fundamental due to vibration of the oxygen bridge bond [35,40,41], and a further 901 cm^{-1} shift, respectively. An output coupler coating specifically designed for the wavelengths of interest would substantially reduce the generation of competing wavelengths. Improvement of the maximum diode-to-third-Stokes conversion efficiency from $\sim 1.3\%$ to 2%–3% might be expected from this setup with higher (optimized) output coupling for the third-Stokes wavelengths.

In intracavity cascaded Raman lasers, heat is deposited in the crystal after the generation of any Stokes-shifted beam, and the thermal lens strength depends on the output power, such that high power Raman lasers can exhibit significant thermal aberrations [39]. Nevertheless, Raman beam cleanup at each conversion step is expected to compensate thermal lensing for improved beam quality at higher Stokes [42]. Measurements of beam quality factors were performed at maximum power, with third-Stokes spectral linewidth of 46 pm FWHM (instrument limited) at 1730 nm and 1 W of output power, and all are depicted in Fig. 9. While near diffraction-limited propagation ($M^2 < 1.01$) of the 1730 nm Raman laser beam was measured, $M^2 < 2.1$ was measured for the fundamental-, first- and second-Stokes-shifted

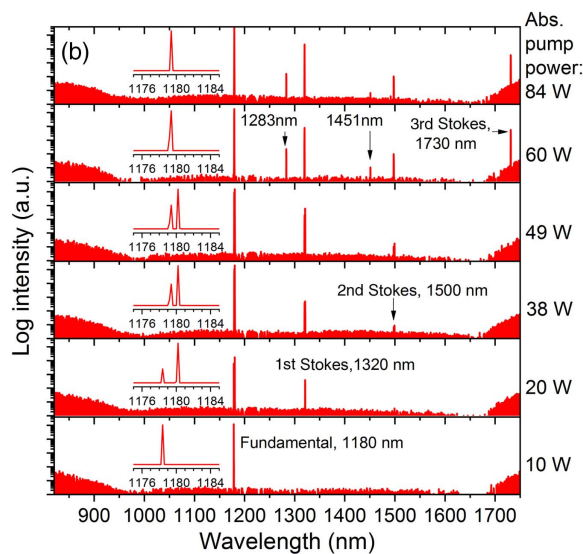
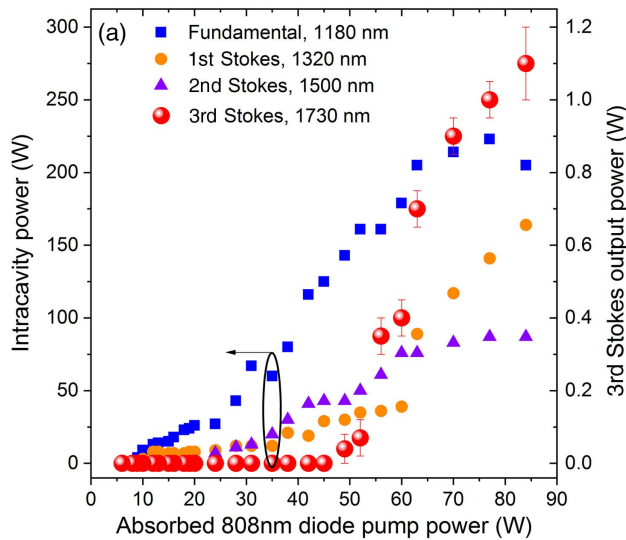


Fig. 8. (a) Power transfer of the third-Stokes Raman laser (red spheres); and intracavity power of the fundamental (blue squares), first-Stokes (orange circles), and second-Stokes (purple triangles). (b) Evolution of the emission spectra of the Raman laser taken with 0.2 nm resolution.

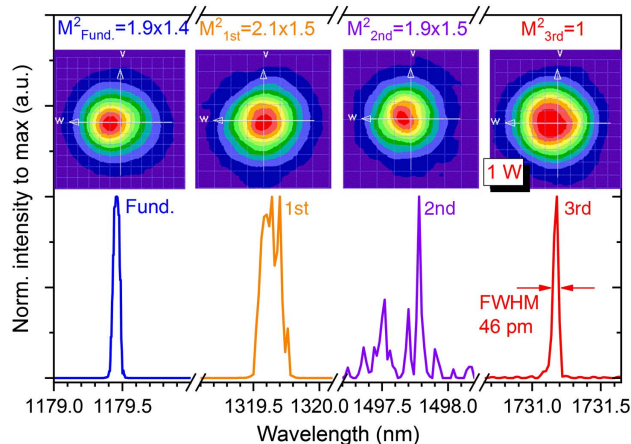


Fig. 9. Spectra of the cascaded Raman lasers collected by an optical spectrum analyzer with 50 pm resolution limit, with 1 W third-Stokes output power. Insets: spatial profiles of the filtered output beams at the fundamental and Raman wavelengths.

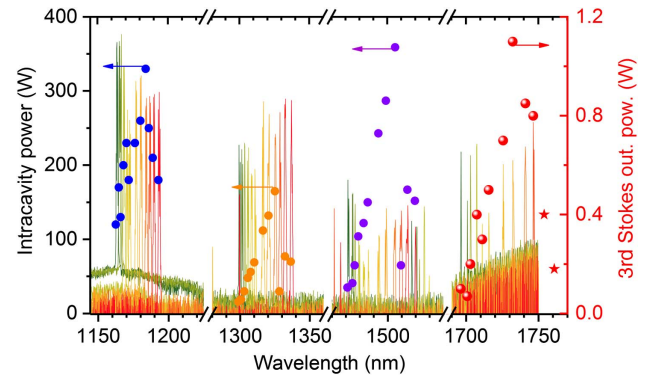


Fig. 10. Tuning of the fundamental and the cascaded Raman laser for an absorbed diode pump power of 84 W and corresponding log-intensity emission spectra (varying from green to red for increasing fundamental wavelength) measured with 0.2 nm resolution. Red stars: calculated wavelength as out of range of the optical spectrum analyzer.

lasers. The SDL (fundamental) was optimized for high intracavity power at the cost of slightly higher M^2 to maintain a good overlap with the pump focus; however, the intracavity-pumped Raman laser does not require pumping with a single transverse mode for high-brightness beams, as it can leverage the intracavity Raman beam cleanup effect.

Non-continuous wavelength tuning of the third-Stokes laser was performed via rotation of the BRF coupled with the 50 μm thick etalon filter in order to achieve narrow linewidth with FWHM ~ 1 nm. Figure 10 shows the tuning curve and spectra of the cascaded Raman laser collected at maximum pump power. The third-Stokes laser varied from 1695.2 nm to ~ 1761 nm while tuning the fundamental in the 1163–1193.2 nm range. Simultaneously, the first- and second-Stokes fields were tuned over 1299.2–1336.8 nm and 1471.4–1519.8 nm, respectively. Third-Stokes laser emission with output power of 1.1 W occurred at 1732.2 nm when the fundamental was tuned to 1180.4 nm. Note that the last two data points in the third-Stokes tuning curve, ~ 1754 nm and ~ 1761 nm, were calculated from the second-Stokes data, as they were out of range of our spectrometer (but detected by the power meter). The tuning of the oscillation wavelength of the SDL was limited by the free spectral range of the BFR, such that even broader tuning could be achieved with the use of a thinner BRF, or, alternatively, a multi-stage birefringent plate (Lyot filter) to simultaneously deliver narrow linewidth and broad continuous tuning.

3. CONCLUSION

We have successfully addressed a performance gap in high-power semiconductor laser spectral coverage via intracavity Raman conversion in an InGaAs SDL. The laser produced watt-level, broadly tunable output at 1.7 μm , thus extending the emission of SDL systems to the region between those based on InGaAsP (up to 1.6 μm) and GaSb (down to 1.9 μm) for the first time.

Frequency conversion from the fundamental wavelength was achieved via multiple (cascaded) Stokes shifts in KGW. Maximum output power of 17.3, 6.1, 1.1, and 1.1 W was produced at the fundamental (1.18 μm), first- (1.32 μm), second- (1.50 μm), and third-Stokes (1.73 μm), respectively, with maximum tuning ranges of 30 nm, 41 nm, 48 nm, and 65 nm.

With this work, we have demonstrated a platform laser technology that takes well-developed InGaAs-based SDLs and provides spectral coverage and high performance in the near-IR water transmission windows using commercially available components.

Finally, to the best of our knowledge, this is the first CW third-Stokes crystalline Raman laser and the longest wavelength from an SDL via Raman conversion. We also demonstrate the first SDL-pumped anti-Stokes laser. Customized mirror coatings to increase the output coupling at the third-Stokes and to suppress parasitic laser oscillation at unwanted Raman modes are expected to lead to improvements in efficiency and, therefore, output power.

Funding. Engineering and Physical Sciences Research Council (EPSRC) (EP/I022791/1); H2020 European Research Council (ERC) (278389); Fraunhofer UK Ltd.; Royal Academy of Engineering.

Acknowledgment. Data related to this publication have been made available at the University of Strathclyde data repository [43].

REFERENCES

- G. M. Gibson, B. Sun, M. P. Edgar, D. B. Phillips, N. Hempler, G. T. Maker, G. P. A. Malcolm, and M. J. Padgett, "Real-time imaging of methane gas leaks using a single-pixel camera," *Opt. Express* **25**, 2998–3005 (2017).
- M.-C. Amann, T. M. Bosch, M. Lescure, R. A. Myllylä, and M. Rioux, "Laser ranging: a critical review of usual techniques for distance measurement," *Opt. Eng.* **40**, 10–19 (2001).
- A. F. Fercher, W. Drexler, C. K. Hitzinger, and T. Lasser, "Optical coherence tomography—principles and applications," *Rep. Prog. Phys.* **66**, 239–303 (2003).
- B. W. Tilma, Y. Jiao, J. Kotani, B. Smalbrugge, H. P. M. M. Ambrosius, and E. A. J. M. Bente, "Integrated tunable quantum-dot laser for optical coherence tomography in the 1.7 μm wavelength region," *IEEE J. Quantum Electron.* **48**, 87–98 (2012).
- S. Ishida and N. Nishizawa, "Quantitative comparison of contrast and imaging depth of ultrahigh-resolution optical coherence tomography images in 800–1700 nm wavelength region," *Biomed. Opt. Express* **3**, 282–294 (2012).
- L. Shi, L. A. Sordillo, A. Rodriguez-Contreras, and R. Alfano, "Transmission in near-infrared optical windows for deep brain imaging," *J. Biophoton.* **9**, 38–43 (2016).
- M. Kuznetsov, F. Hakimi, R. Sprague, and A. Mooradian, "Design and characteristics of high-power (<0.5-W CW) diode-pumped vertical-external-cavity surface-emitting semiconductor lasers with circular TEM₀₀ beams," *IEEE J. Sel. Top. Quantum Electron.* **5**, 561–573 (1999).
- M. Guina, A. Rantamäki, and A. Härkönen, "Optically pumped VECSELs: review of technology and progress," *J. Phys. D* **50**, 383001 (2017).
- B. Heinen, T.-L. Wang, M. Sparenberg, A. Weber, B. Kunert, J. Hader, S. W. Koch, J. V. Moloney, M. Koch, and W. Stolz, "106 W continuous-wave output power from vertical-external-cavity surface-emitting laser," *Electron. Lett.* **48**, 516–517 (2012).
- S. Ranta, M. Tavast, T. Leinonen, N. Van Lieu, G. Fetzer, and M. Guina, "1180 nm VECSEL with output power beyond 20 W," *Electron. Lett.* **49**, 59–60 (2013).
- A. R. Albrecht, T. J. Rotter, C. P. Hains, A. Stintz, J. V. Moloney, K. J. Malloy, and G. Balakrishnan, "Multi-watt 1.25 μm quantum dot VECSEL," *Electron. Lett.* **46**, 856–857 (2010).
- J.-M. Hopkins, S. A. Smith, C. W. Jeon, H. D. Sun, D. Burns, S. Calvez, M. D. Dawson, T. Jouthi, and M. Pessa, "0.6 W CW GaInNAs vertical external-cavity surface emitting laser operating at 1.32 μm ," *Electron. Lett.* **40**, 30–31 (2004).
- V.-M. Korpjärvi, T. Leinonen, J. Puustinen, A. Härkönen, and M. D. Guina, "11 W single gain-chip dilute nitride disk laser emitting around 1180 nm," *Opt. Express* **18**, 25633–25641 (2010).
- A. Sirbu, N. Volet, A. Mereuta, J. Lytykäinen, J. Rautiainen, O. Okhotnikov, J. Walczak, M. Wasiaik, T. Czeszanowski, A. Caliman, G. Zhu, V. Iakovlev, and E. Kapon, "Wafer-fused optically pumped VECSELs emitting in the 1310-nm and 1550-nm wavebands," *Adv. Opt. Technol.* **2011**, 209093 (2011).
- A. Sirbu, A. Rantamäki, E. J. Saarinen, V. Iakovlev, A. Mereuta, J. Lytykäinen, A. Caliman, N. Volet, O. G. Okhotnikov, and E. Kapon, "High performance wafer-fused semiconductor disk lasers emitting in the 1300 nm waveband," *Opt. Express* **22**, 29398–29403 (2014).
- D. C. Parrotta, A. J. Kemp, M. D. Dawson, and J. E. Hastie, "Tunable continuous-wave diamond Raman laser," *Opt. Express* **19**, 24165–24170 (2011).
- D. C. Parrotta, W. Lubeigt, A. J. Kemp, D. Burns, M. D. Dawson, and J. E. Hastie, "Continuous-wave Raman laser pumped within a semiconductor disk laser cavity," *Opt. Lett.* **36**, 1083–1085 (2011).
- D. C. Parrotta, A. J. Kemp, M. D. Dawson, and J. E. Hastie, "Multiwatt, continuous-wave, tunable diamond Raman laser with intracavity frequency-doubling to the visible region," *IEEE J. Sel. Top. Quantum Electron.* **19**, 1400108 (2013).
- P. Holl, M. Rattunde, S. Adler, S. Kaspar, W. Bronner, A. Bachle, R. Aidam, and J. Wagner, "Recent advances in power scaling of GaSb-based semiconductor disk lasers," *IEEE J. Sel. Top. Quantum Electron.* **21**, 324–335 (2015).
- H. M. Pask, "The design and operation of solid-state Raman lasers," *Prog. Quantum Electron.* **27**, 3–56 (2003).
- S. H. Ding, X. Y. Zhang, Q. P. Wang, F. F. Su, S. T. Li, S. Z. Fan, Z. J. Liu, J. Chang, S. S. Zhang, S. M. Wang, and Y. R. Liu, "Theoretical and experimental research on the multi-frequency Raman converter with KGd(WO₄)₂ crystal," *Opt. Express* **13**, 10120–10128 (2005).
- A. McKay, O. Kitzler, and R. P. Mildren, "High power tungstate-crystal Raman laser operating in the strong thermal lensing regime," *Opt. Express* **22**, 707–715 (2014).
- O. Lux, S. Sarang, R. J. Williams, A. McKay, and R. P. Mildren, "Single longitudinal mode diamond Raman laser in the eye-safe spectral region for water vapor detection," *Opt. Express* **24**, 27812–27820 (2016).
- D. C. Parrotta, R. Casula, J. Penttinen, T. Leinonen, A. J. Kemp, M. Guina, and J. E. Hastie, "InGaAs-QW VECSEL emitting 1300-nm via intracavity Raman conversion," *Proc. SPIE* **9734**, 973400 (2016).
- R. J. Williams, D. J. Spence, O. Lux, and R. P. Mildren, "High-power continuous-wave Raman frequency conversion from 1.06 μm to 1.49 μm in diamond," *Opt. Express* **25**, 749–757 (2017).
- R. Casula, J.-P. Penttinen, A. J. Kemp, M. Guina, and J. E. Hastie, "1.4 μm continuous-wave diamond Raman laser," *Opt. Express* **25**, 31377–31383 (2017).
- I. V. Mochalov, "Laser and nonlinear properties of the potassium gadolinium tungstate laser crystal KGd(WO₄)₂:Nd³⁺-(KGW:Nd)," *Opt. Eng.* **36**, 1660–1669 (1997).
- R. P. Mildren, D. W. Coutts, and D. J. Spence, "All-solid-state parametric Raman anti-Stokes laser at 508 nm," *Opt. Express* **17**, 810–818 (2009).
- X. Wang, W. Kang, X. Song, P. Xie, N. Zong, and W. Tu, "Theoretical and experimental research on high-order stimulated Raman scattering in KGd(WO₄)₂," *Opt. Commun.* **385**, 9–14 (2017).
- E. Kantola, T. Leinonen, S. Ranta, M. Tavast, and M. Guina, "High-efficiency 20 W yellow VECSEL," *Opt. Express* **22**, 6372–6380 (2014).
- Z. Liao, "Semiconductor wafer bonding via liquid capillarity," *Appl. Phys. Lett.* **77**, 651–653 (2000).
- H. M. Pask and J. A. Piper, "Raman lasers," in *Handbook of Solid-State Lasers* (Elsevier, 2013), pp. 493–524.
- J. A. Caird, S. A. Payne, P. Randall Staver, A. J. Ramponi, L. L. Chase, and W. F. Krupke, "Quantum electronic properties of the Na₃Ga₂Li₅F₁₂:Cr³⁺ laser," *IEEE J. Quantum Electron.* **24**, 1077–1099 (1988).
- A. S. Grabtchikov, A. N. Kuzmin, V. A. Lisinetskii, G. I. Ryabtsev, V. A. Orlovich, and A. A. Demidovich, "Stimulated Raman scattering in Nd:KGW laser with diode pumping," *J. Alloys Compd.* **300**, 300–302 (2000).
- L. Macalik, J. Hanuza, and A. A. Kaminskii, "Polarized infrared and Raman spectra of KGd(WO₄)₂ and their interpretation based on normal coordinate analysis," *J. Raman Spectrosc.* **33**, 92–103 (2002).
- J. J. Neto, C. Artlett, A. Lee, J. Lin, D. Spence, J. Piper, N. U. Wetter, and H. Pask, "Investigation of blue emission from Raman-active crystals: its origin and impact on laser performance," *Opt. Mater. Express* **4**, 889–902 (2014).

37. R. J. Williams, O. Kitzler, Z. Bai, S. Sarang, H. Jasbeer, A. McKay, S. Antipov, A. Sabella, O. Lux, D. J. Spence, and R. P. Mildren, "High power diamond Raman lasers," *IEEE J. Sel. Top. Quantum Electron.* **24**, 1602214 (2018).
38. V. G. Savitski, I. Friel, J. E. Hastie, M. D. Dawson, D. Burns, and A. J. Kemp, "Characterization of single-crystal synthetic diamond for multi-watt continuous-wave Raman lasers," *IEEE J. Quantum Electron.* **48**, 328–337 (2012).
39. J. A. Piper and H. M. Pask, "Crystalline Raman lasers," *IEEE J. Sel. Top. Quantum Electron.* **13**, 692–704 (2007).
40. A. Senthil Kumaran, S. Moorthy Babu, S. Ganesamoorthy, I. Bhaumik, and A. K. Karnal, "Crystal growth and characterization of KY(WO₄)₂ and KGd(WO₄)₂ for laser applications," *J. Cryst. Growth* **292**, 368–372 (2006).
41. D. Kasprowicz, T. Runka, A. Majchrowski, E. Michalski, and M. Drozdowski, "Vibrational properties of Nd³⁺, Eu³⁺, Er³⁺ and Ho³⁺ doped KGd(WO₄)₂ single crystals studied by Raman scattering method," *Phys. Procedia* **2**, 539–550 (2009).
42. J. T. Murray, W. L. Austin, and R. C. Powell, "Intracavity Raman conversion and Raman beam cleanup," *Opt. Mater.* **11**, 353–371 (1999).
43. <http://dx.doi.org/10.15129/c0974aad-0284-4980-9c2f-690923708203>.